Electronic Supplementary Information

W_2C Nanorods with Various Amounts of Vacancy Defects：Determination of Catalytic Active Sites in Hydrodeoxygenation of Benzofuran

Rong Liu,[a] Min Pang,[b] Xiaozhen Chen,[b] Chuang Li,[b] Chunjian Xu, *, [a] Changhai Liang *, [b]

[a] State Key Laboratory of Chemical Engineering, Chemical Engineering Research Center, and School of Chemical Engineering and Technology, Tianjin University, Tianjin 300072, China

[b] Laboratory of Advanced Materials and Catalytic Engineering, School of Chemical Engineering, Dalian University of Technology, Dalian 116024, China

Corresponding Author: cjxu@tju.edu.cn, changhai@dlut.edu.cn

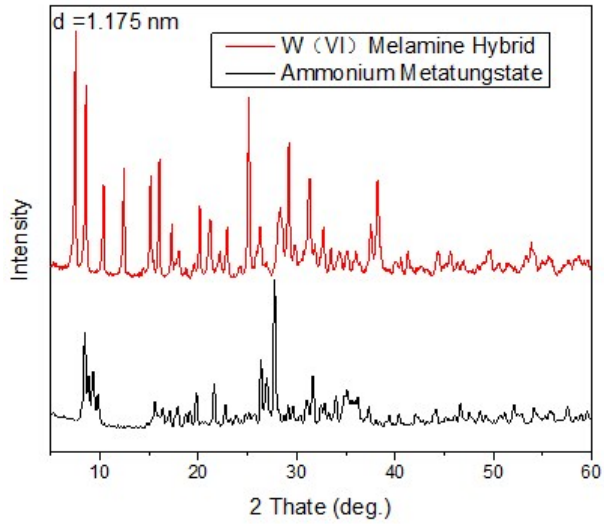

Figure S1.XRD patterns of $(NH_4)_6$ $H_2W_{12}O_{40}$*nH_2O and as-synthesized organic- inorganic hybrid

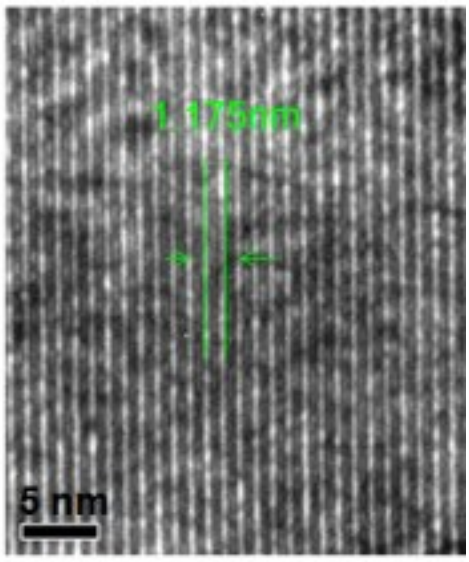

Figure S2. High-resolution TEM images of the hybrid

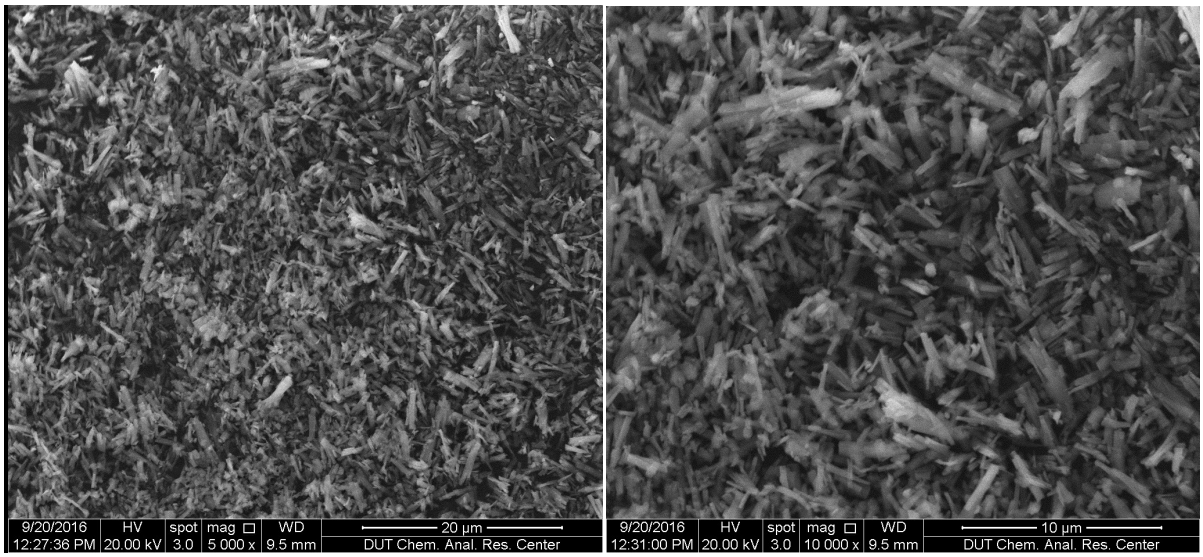

Figure S3.SEM images of the Hybrid Nanorods.

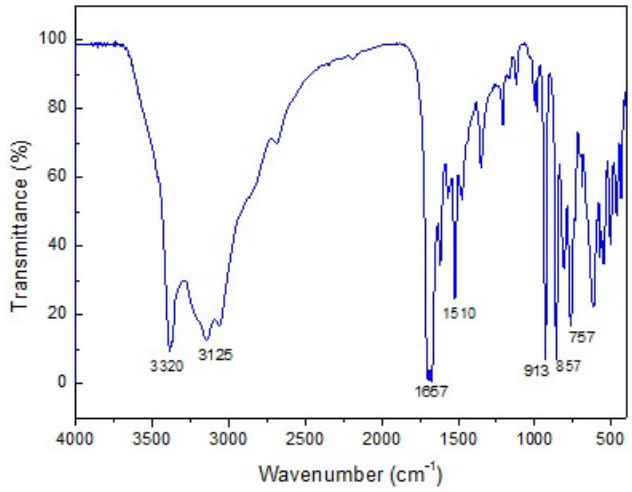

Figure S4.IR spectrum of as-synthesized organic-inorganic hybrid.

The hybrid components are well confirmed by the characteristic absorption peaks at 3320, 3125, 1657 and 1510 cm^{-1} (melamine) and 913,867 and 757 cm^{-1} (tungstate).

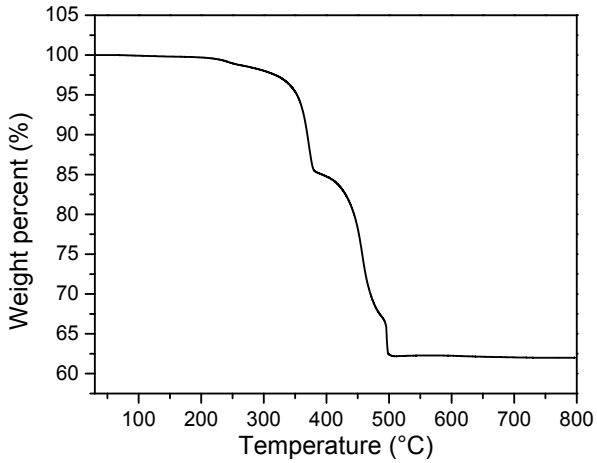

Figure S5.TGA curve (under air flow) of the as-synthesized organic- inorganic hybrid.

The final weight is reduced to 62% of its initial weight. The large weight loss from 350 to 500 °C is due to the sublimation or decomposition of melamine in the hybrid. The temperature is higher than the sublimation point of melamine (~300 °C).

Table S1. Element content of the Hybrid

	W (wt%)	O (wt%)	N (wt%)	C (wt%)	H (wt%)
Content	49.2[a]	16.3[b]	23.0	9.6	1.9

a: Dtermined by TG analysis, b:O(wt%)=1-W(wt%)-N(wt%)-C(wt%)-H(wt%)

The element content of the hybrid is in good agreement with the stoichiometric composition $(C_3H_7N_6)_8W_{12}O_{40}*4H_2O*4C_3H_6N_6$. The attached$4C_3H_6N_6$ may be melamine entrained during the precipitation process because some of the unreacted excess melamine can also precipitate as temperature decreases fast.

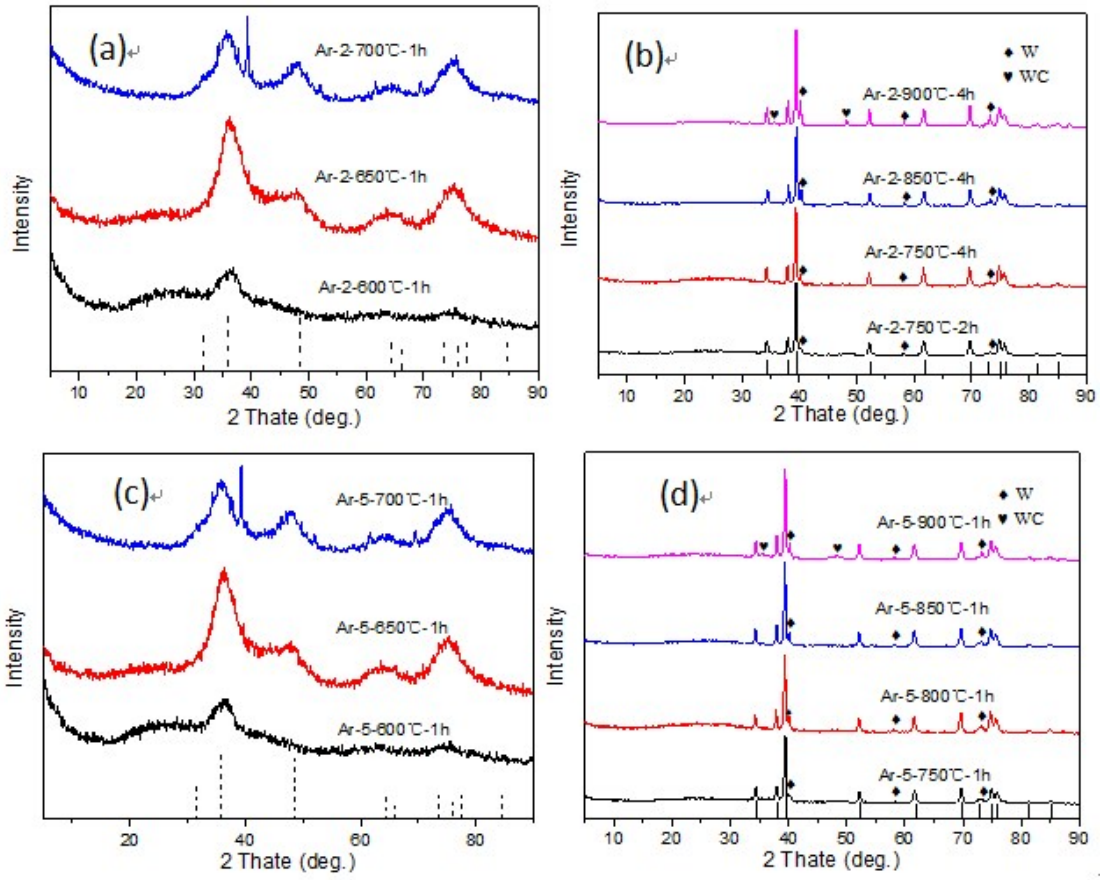

Figure S6. XRD patterns of the samples originating from the heat treatment of the W(VI) −melamine hybrid at different conditions. The standard patterns of WN (PDF# 25-1256) andW_2C (PDF# 35-0776) are shown (dashed lines) at the bottom on the left and right, respectively.

Table S2. Phase Identifications; W, C, and N Contents; W/C and N/W Molar Ratios and Surface Areas of the Products obtained at different conditions

Sample	Phase[a]	N content (wt%)	C content (wt%)	W content[b] (wt%)	W/C (molar ratio)	N/W (molar ratio)	S_{BET}[c] (m^2/g)
W-2-650℃-1h	W_2C+WC_xN_y	4.00	2.99	90.6	2.0	0.58	
W-2-700℃-1h	W_2C+WC_xN_y	3.20	3.36	91.7	1.8	0.46	
Ar-2-750℃-1h	W_2C	1.08	3.11	94.8	2.0	0.14	18.52
Ar-2-800℃-1h	W_2C+W	0.55	2.92	96.1	2.1	0.07	18.42
Ar-2-850℃-1h	W_2C+W	0.41	3.15	96.2	2.0	0.06	16.96
Ar-2-900℃-1h	W_2C+W+WC	0.22	2.97	96.7	2.1	0.03	14.67
Ar-5-750℃-1h	W_2C+W	1.49	3.00	94.2	2.1	0.20	18.27
Ar-5-800℃-1h	W_2C+W	0.49	2.99	96.0	2.1	0.07	17.81
Ar-5-850℃-1h	W_2C+W	0.33	2.96	96.4	2.1	0.04	16.82
Ar-2-750℃-4h	W_2C+W	0.44	2.94	96.1	2.1	0.06	17.85
Ar-2-750℃-1h-H_2	W_2C+W	0.10	2.53	97.2	2.5	0.01	17.25

[a]Determined by XRD analysis. [b]Data obtained from thermogravimetry conducted in air.[c]Specific surface area was calculated by the Brunauer −Emmett −Teller method.

Table S3. The relative catalytic activities of each catalyst (The catalytic activityR_{H2}) of Ar-2-750°C-1h was taken as the reference 1) at different temperatures and their W phase contents and particle sizes in XRD

Temperature /℃	320	330	340	350	W phase content in XRD /(%)[a]	Particle Size /(nm)[b]
Ar-2-900℃-1h	2.02		2.23	2.05	2.91	27.10
Ar-2-750℃-1hH2	1.91		2.22	1.99	2.77	30.10
Ar-5-850℃-1h	1.88		2.05	1.87	3.43	28.30
Ar-5-800℃-1h	1.79	1.75	1.81	1.58	4.21	26.20
Ar-2-850℃-1h	1.69		1.80	1.63	2.28	28.40
Ar-2-750℃-4h	1.51		1.59	1.45	2.12	29.10
Ar-2-800℃-1h	1.09		1.19	1.05	1.71	25.80
Ar-5-750℃-1h	1.03		1.06	0.97	1.59	27.20
Ar-2-750℃-1h	1.00	1.00	1.00	1.00	1.00	29.00

[a]The molar fraction x of W in a W_2C -WC -W mixture was calculated from XRD patterns as

$$x = \frac{S_1}{S_1 + S_2 + S_3}$$

where S_1, S_2, and S_3 are the peak areas of the most intense reflections of W_2C, WC, and W, respectively.

[b]The average size of tungsten carbide particles was evaluated by the Scherrer formula.

Table S4. The catalytic activities of catalysts (Ar-2-750℃-1hH_2 and Ar-2-900℃-1h) placed in air for days, comparing to the fresh.

Catalyst	R_{DO}[b]	R_{H2}[c]
Ar-2-750℃-1hH_2 45days	0.9	47.6
Ar-2-750℃-1hH_2 fresh	10.9	115.8
Ratio[a]	9%	41%

Catalyst	R_{DO}	R_{H2}
Ar-2-900℃-1h 90days	0.6	21.0
Ar-2-900℃-1h fresh	9.3	116.2
Ratio	6%	18%

Reaction condition：

340℃, 4MPa, W/F=3.044 $g_{cat}/(g_{BF}\cdot h^{-1})$, H_2/oil volume ratio=1000:1

[a]the ratio of used comparing to fresh.

[b]R_{DO} Unit: 10^{11} deoxygenated molecules $cm_{cat}^{-2}s^{-1}$

[c] R_{H2} Unit: 10^{11} reacted H_2 molecules $cm_{cat}^{-2}s^{-1}$

Table S5. Apparent Activation Energies and Bond Dissociation Energies

Reacted Bond	C=C	C-O	C_{ar}-O	H_2	C-C	C-C_6H_{11}	HO-C_6H_{11}
Apparent Activation Energies (kJ/mol)	68.49	86.56	134.45	84.77	96.44		
Bond Dissociation Energies[1] (kJ/mol)		255	464		325	377	399

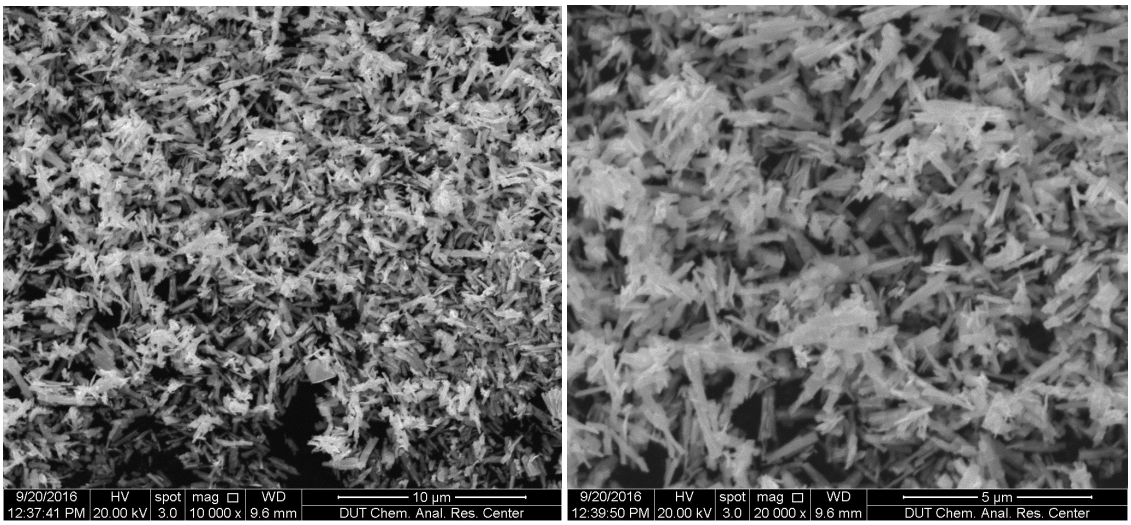

Figure S7.SEM images of Ar-2-750℃-1h

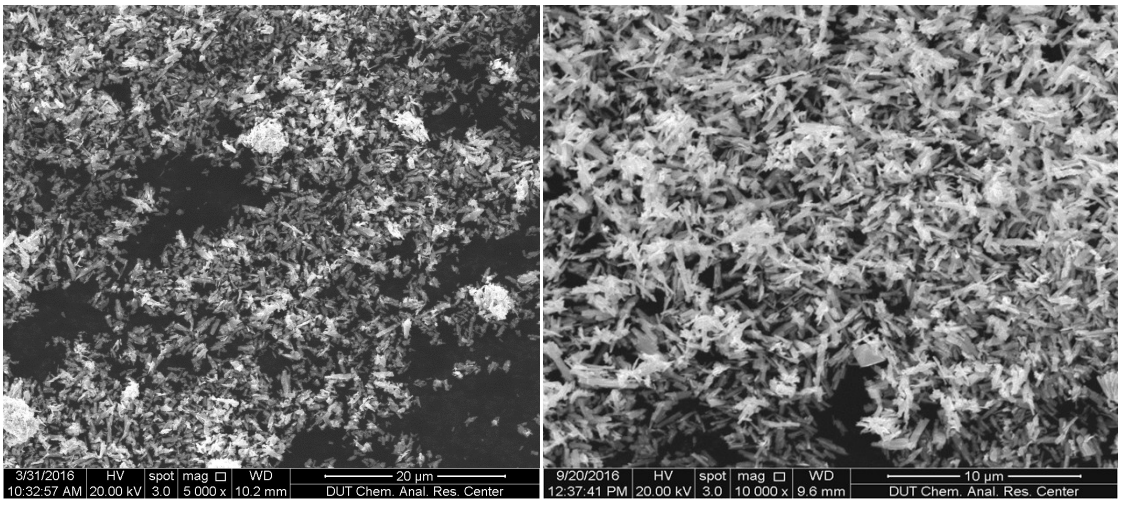

Figure S8.SEM images of Ar-2-750℃-4h

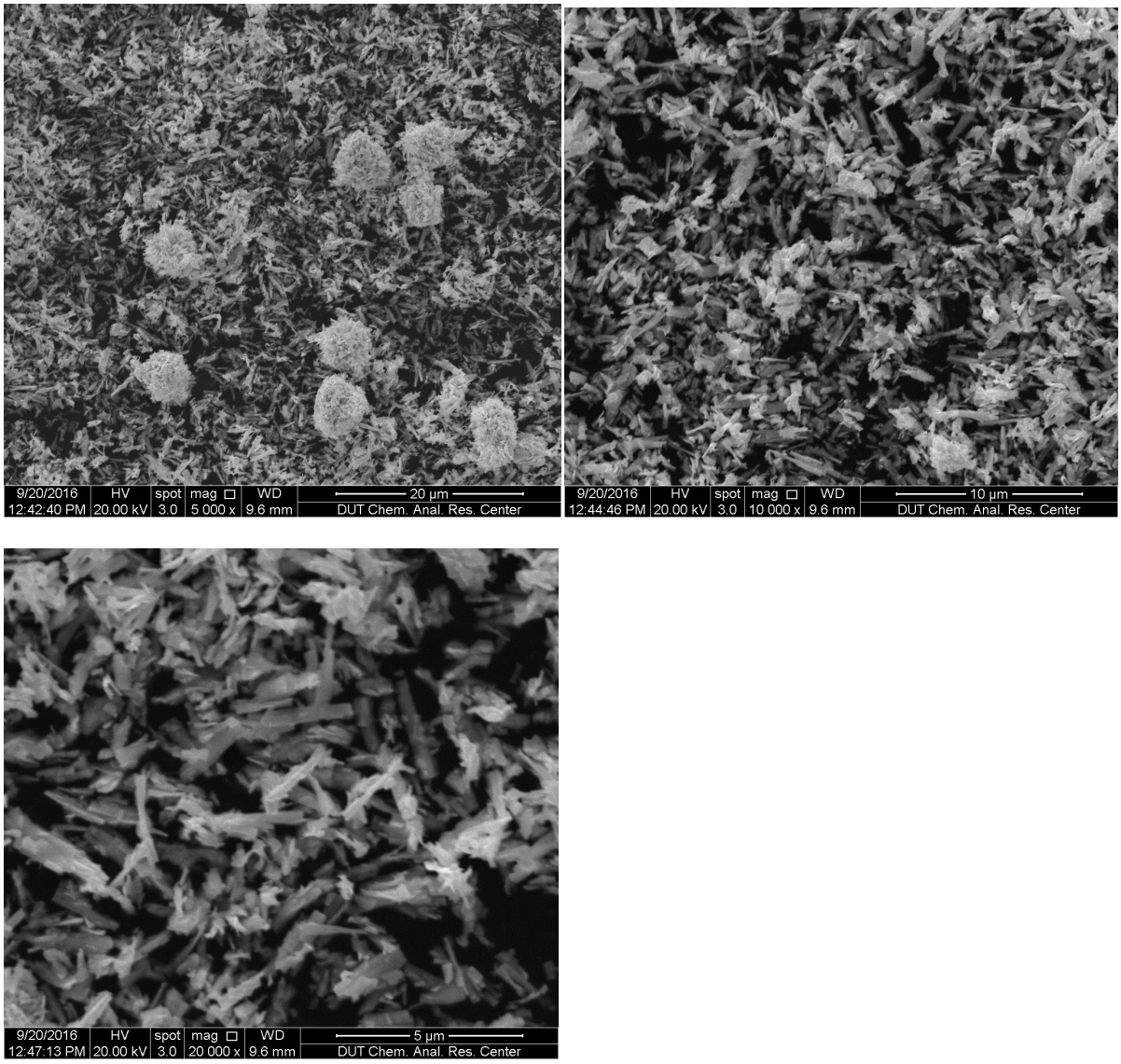

Figure S9.SEM images of Ar-2-900℃-1h

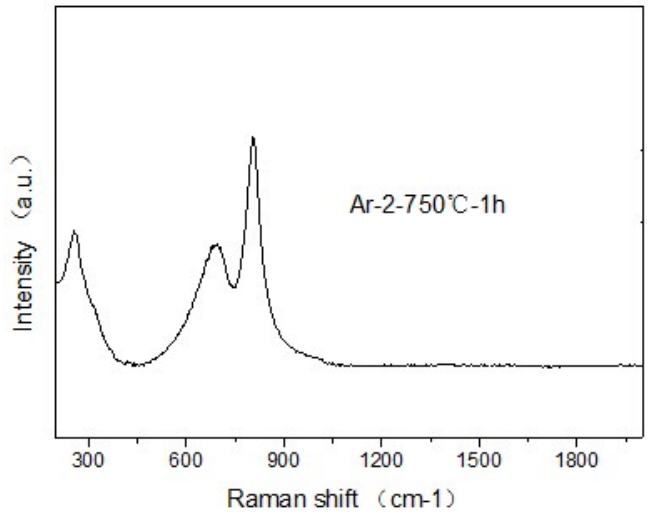

Figure S10. Raman spectra of W_2C (Ar-2-750℃-1h) synthesized from the organic- inorganic hybrid.

It is confirmed that there is no residual carbon in W_2C nanorods, because the characteristic D-band (~1345 cm^{-1}) and G-band (~1589 cm^{-1}) of carbon are absent in the Raman spectrum of W_2C nanorods. G-band is corresponding to the vibration of sp^2 hybridized carbon in the two-dimensional graphite for ordered carbon species and the D-band was highly sensitive to amorphous carbon or defects in the G-band.

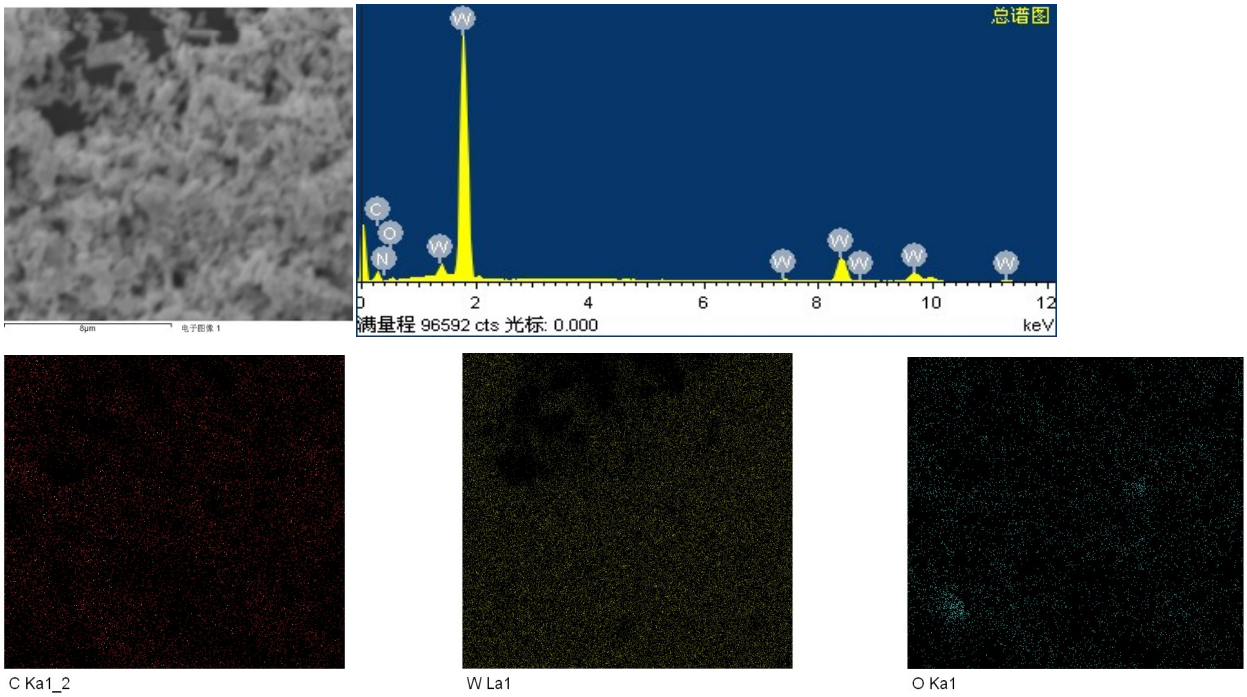

Figure S11. SEM Energy dispersive spectroscopy and elemental mapping images of W_2C nanorods(Ar-2-750℃-1h).

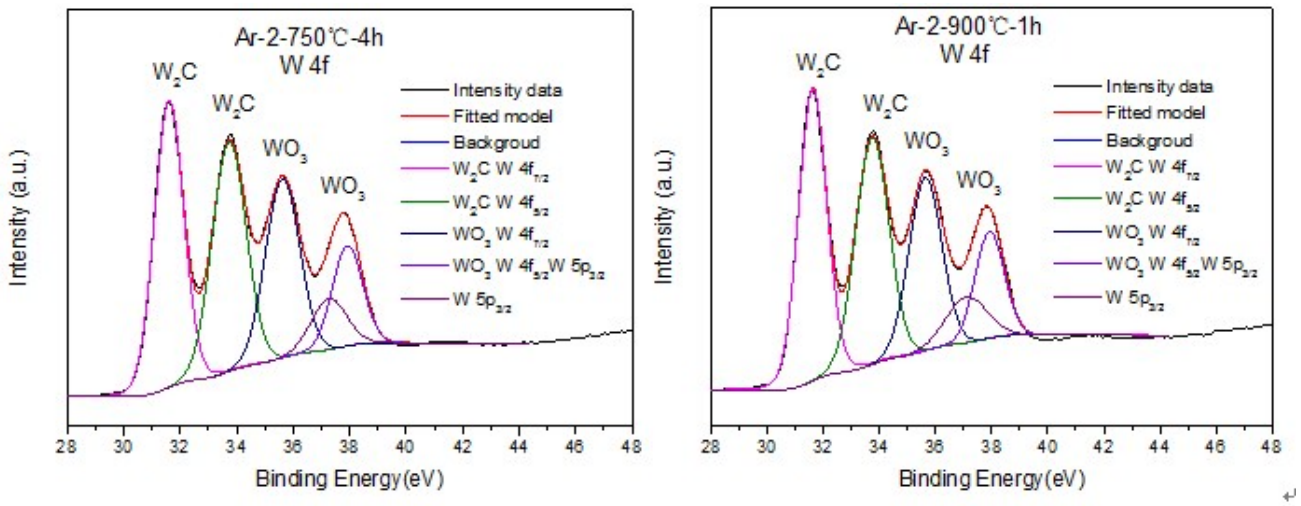

Figure S12.XPS W 4f spectra of Ar-2-750°C-4h and Ar-2-900°C-1h.

The W-4f region shows peaks at 31.7 eV (W $4f_{7/2}$), 33.8 eV (W $4f_{5/2}$) and 37.2 eV (W $5p_{3/2}$), corresponding to W_2C. Peaks observed at 35.97eV (W $4f_{7/2}$) and 37.9 eV (W $4f_{5/2}$) are related to WO_3 (W^{6+}) (fig), which indicates that some part of surface W_2C was oxidized in air after preparation. The tungsten carbide/oxide surface ratios in the three samples were all estimated to be about 64:36.The W $5p_{3/2}$ line shape and peak area relative to W$4f_{7/2}$ were used to subtract W 5p3/2 contributions from the W 4f spectra of the oxide-containing W_2C surfaces.

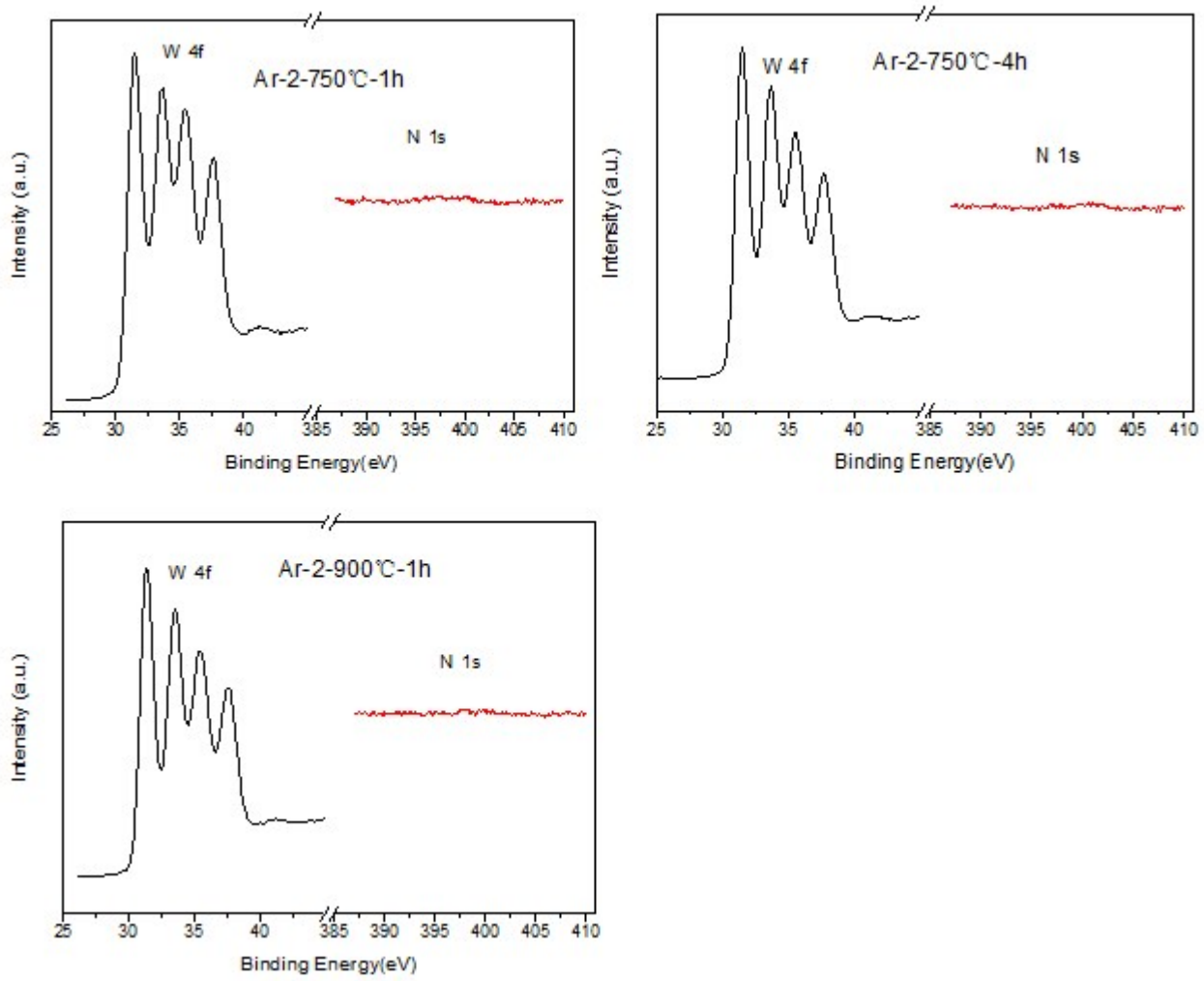

Figure S13.XPS comparison of the C 1s and W 4f signals. There were no sharp peaks in N 1s.

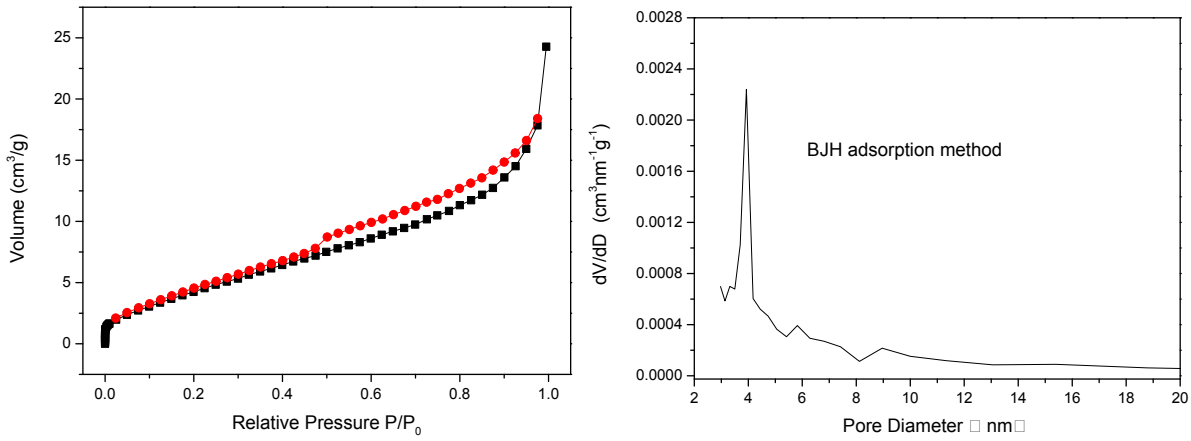

Figure S14. N_2 sorption isotherms and pore diameter distribution of W_2C nanorods (Ar-2-750°C-1h).

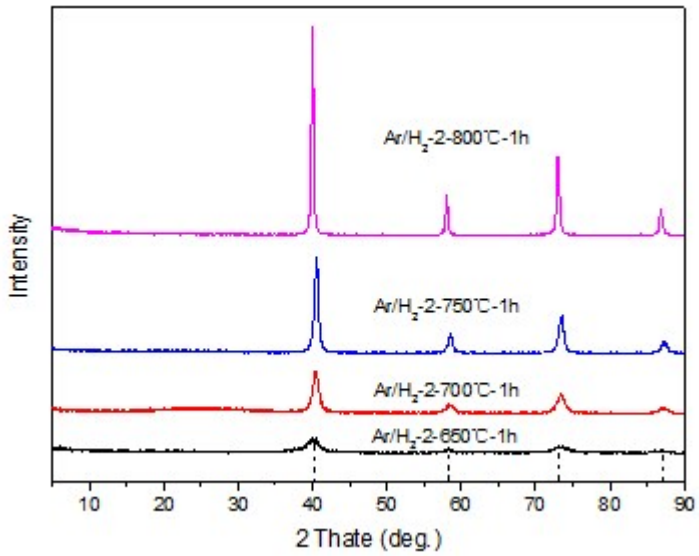

Figure S15. XRD patterns of products obtained in the mixture of argon and H_2.

The standard pattern of W (PDF# 04-0806) is shown (dashed lines) at the bottom.

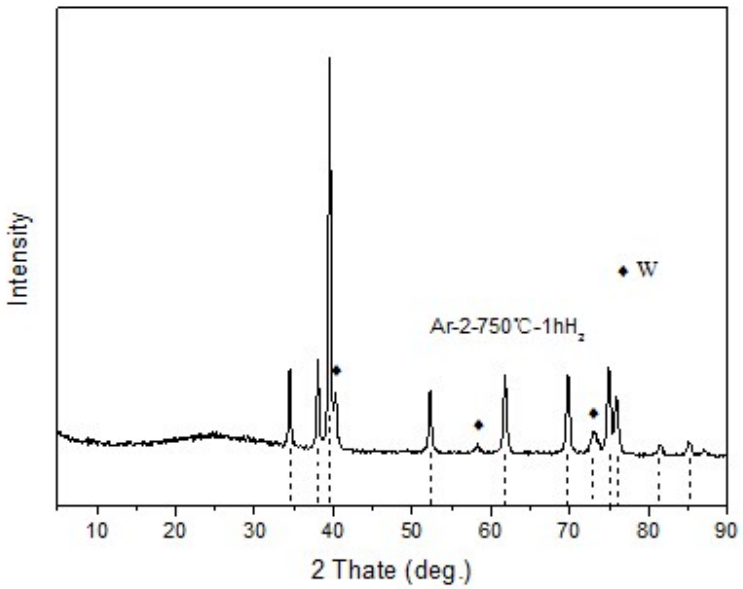

Figure S16. XRD patterns of Ar-2-750°C-1hH_2.

The standard pattern of W_2C (PDF# 35-0776) is shown (dashed lines) at the bottom.

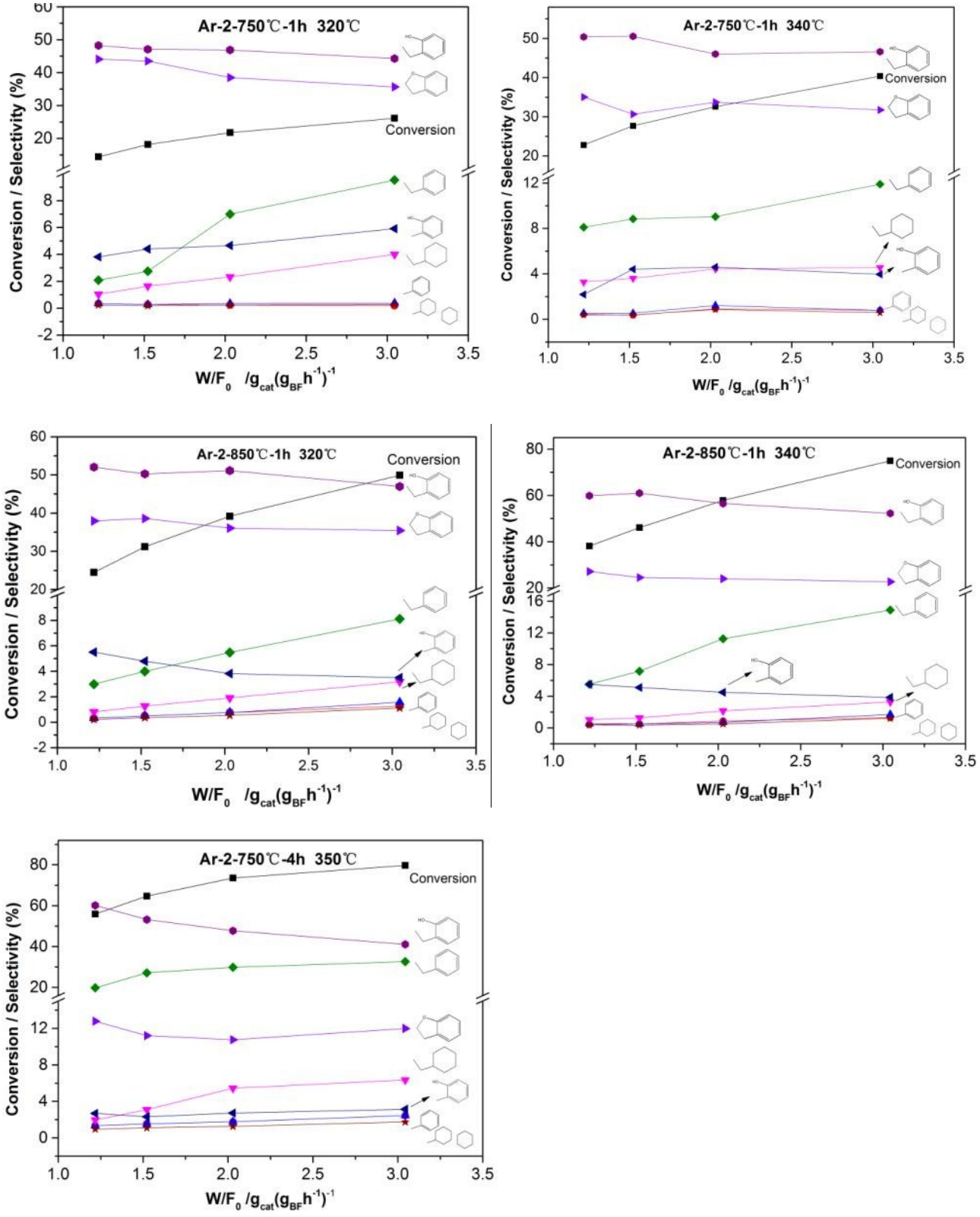

Figure S17. Conversion and selectivity as a function of contact time at different temperatures on a variety of W_2C catalysts respectively.

As increasing the contact time, the reaction conversion increases, and the selectivity of the deoxygenation product is obviously enhanced (ethylbenzene is the main deoxygenation product).

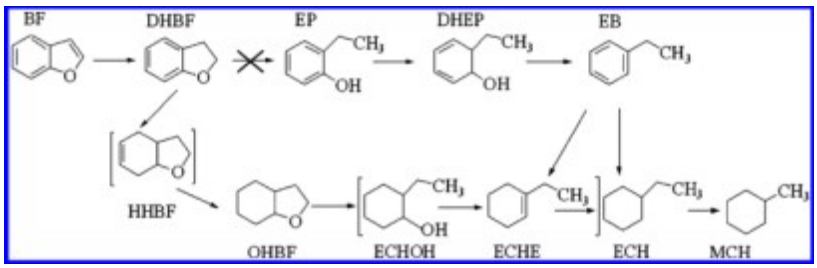

Scheme S1. The reaction pathway of hydrodeoxygenation of benzofuran on noble metal catalysts Pt and Pd.[2]

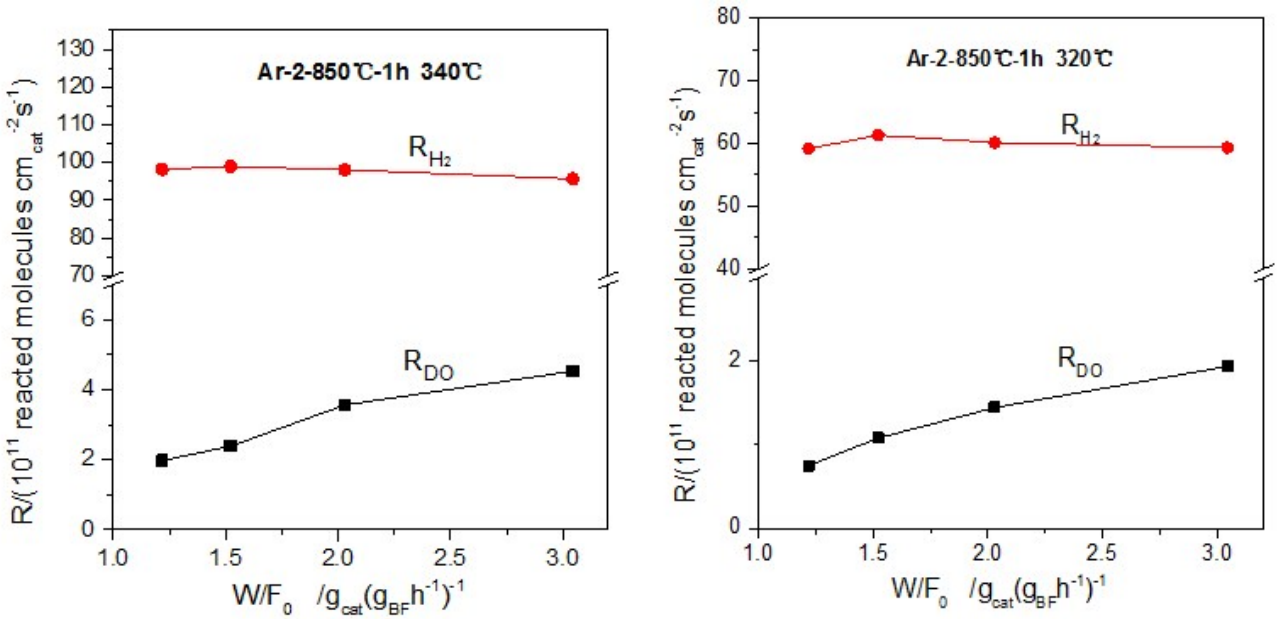

Figure S18. The overall hydrogen reaction rate (R_{H2}) and deoxygenation rate （R_{DO}）withdifferent contact timesat different temperatures on Ar-2-850℃-1h.

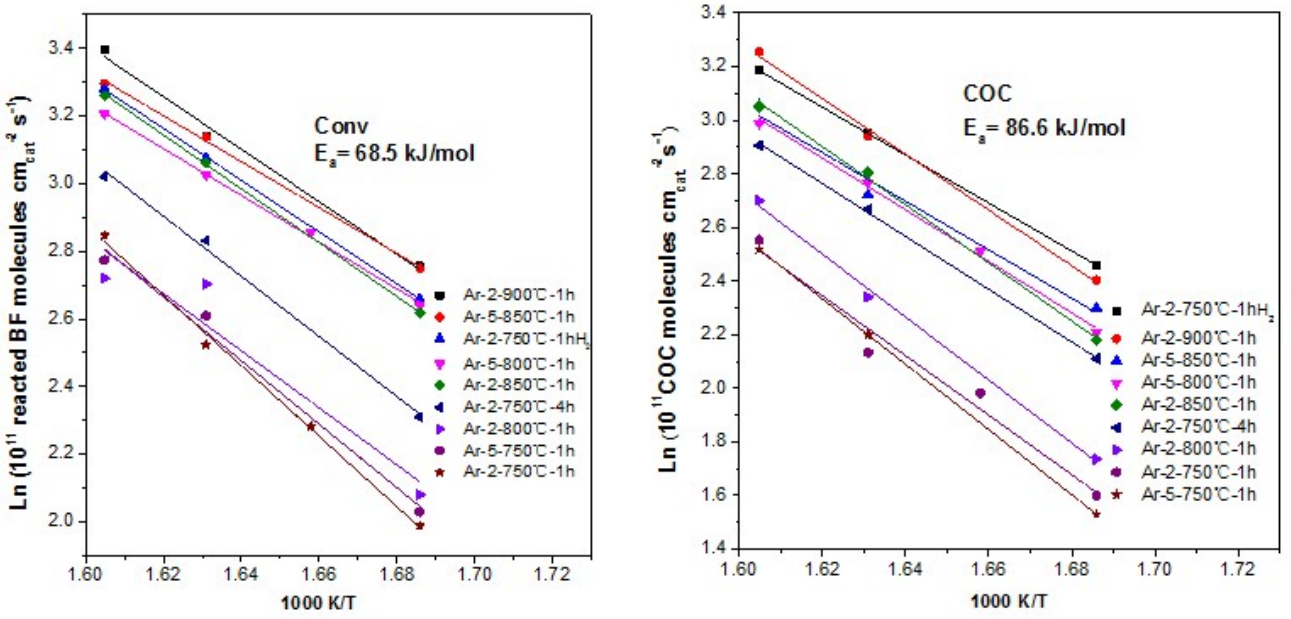

Figure S19. Arrhenius plots for R_{Conv} and R_{COB} on different W_2C catalysts.

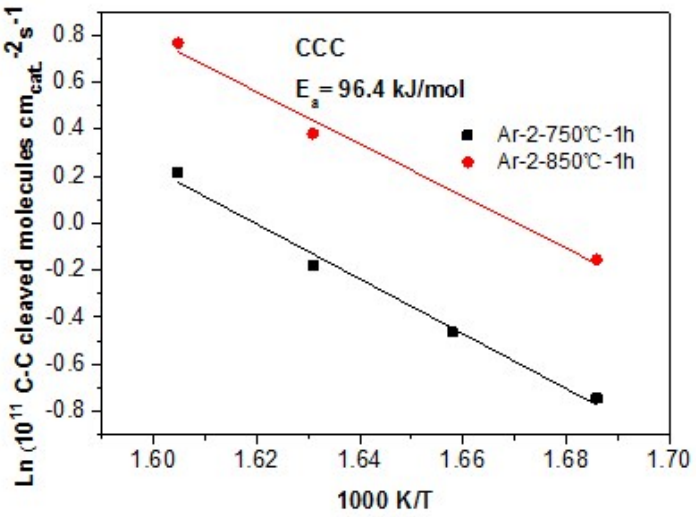

Figure S20. Arrhenius plots for R_{CCC} on Ar-2-750°C-1h and Ar-2-850°C-1h.

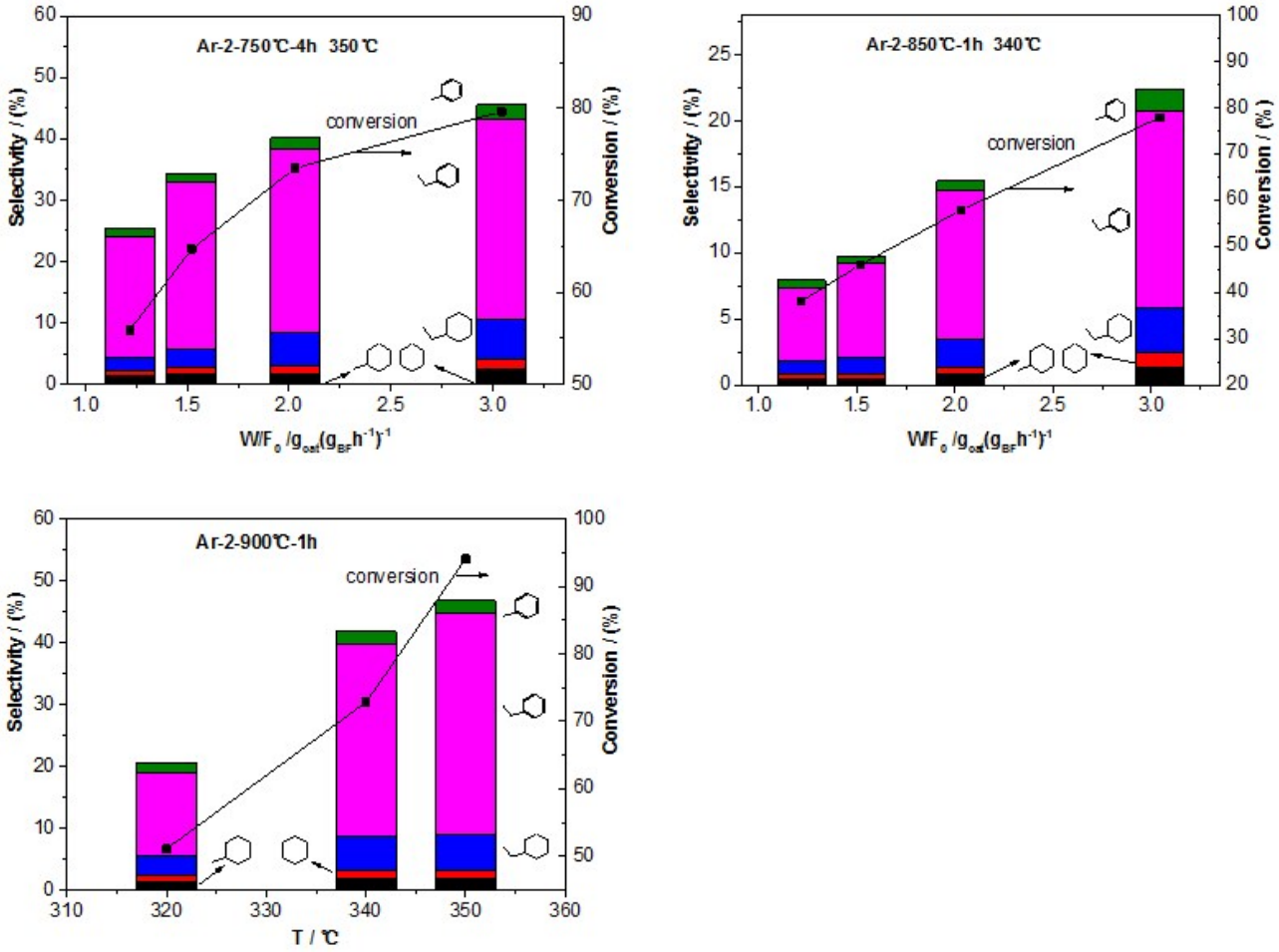

Figure S21. Selectivity for hydrocarbons. The main hydrocarbon product is ethylbenzene.

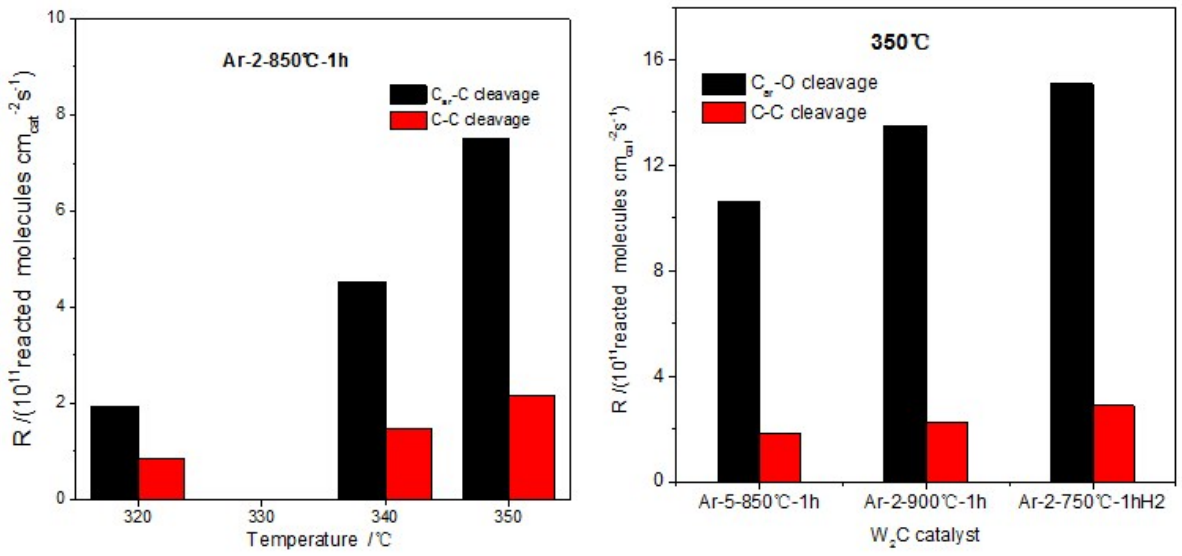

Figure S22.R_{DO}comparing with R_{COC}.

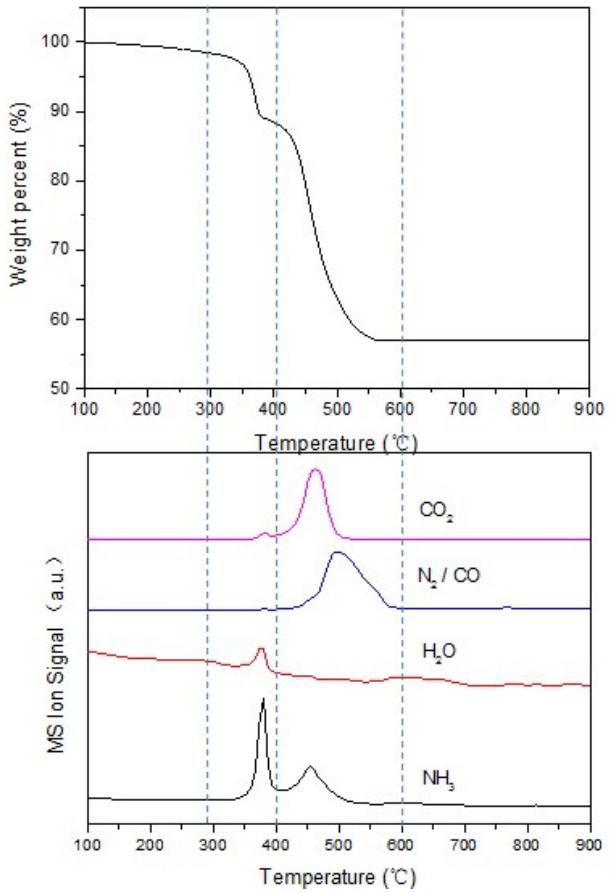

Figure S23. (a) TG −DTG curves (obtained in Argon) of the W(VI) −melamine hybrid. The large weight loss from 350 to 500 °C is due to the sublimation or decomposition of melamine in the hybrid. (b) Mass spectra of the gases evolvedduring the thermal decomposition of the hybrid inArgon. The mass spectra have been divided into four distinct regions. Compositions of the species are given over the curves.

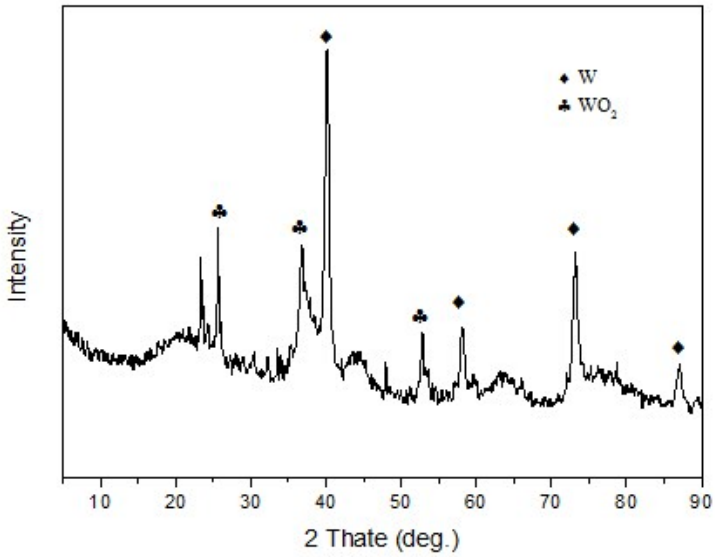

Figure S24.XRD pattern of the sample resulting from the heat treatment of a mechanical mixture of $(NH_4)_6\ H_2W_{12}O_{40}$*$nH_2O$ and melamine at 800 °C in Argon for 1 h.

The diffractions are typical of metallic tungsten and tungsten oxides.

Figure S25. TEM, HRTEM and Fast Fourier transform (FFT) images of W_2C with various amounts of defects obtained at different condition.

Some of them are marked with line profile or green color to display the vacancy defects.Observed by HRTEM, we got the order of the numbers of vacancies by counting the numbers of vacancies on multiple HRTEM images (larger than 3000 square nanometers for each sample), the statistical average numbers of carbon vacancies per square nanometers of the products were obtained: Ar-2-750°C-1hH_2 (2.5 vacancies/nm^2), Ar-2-900°C-1h (2.6 vacancies/nm^2) > Ar-5-800°C-1h (1.7 vacancies/nm^2), Ar-2-750°C-4h (1.6 vacancies/nm^2) > Ar-2-750°C-1h (1.1 vacancies/nm^2), which is consistent with the order of R_{H2}. The number of vacancies and the level of activity were nearly linear positively correlated.

Large amount of TEM and HRTEM images are listed below:

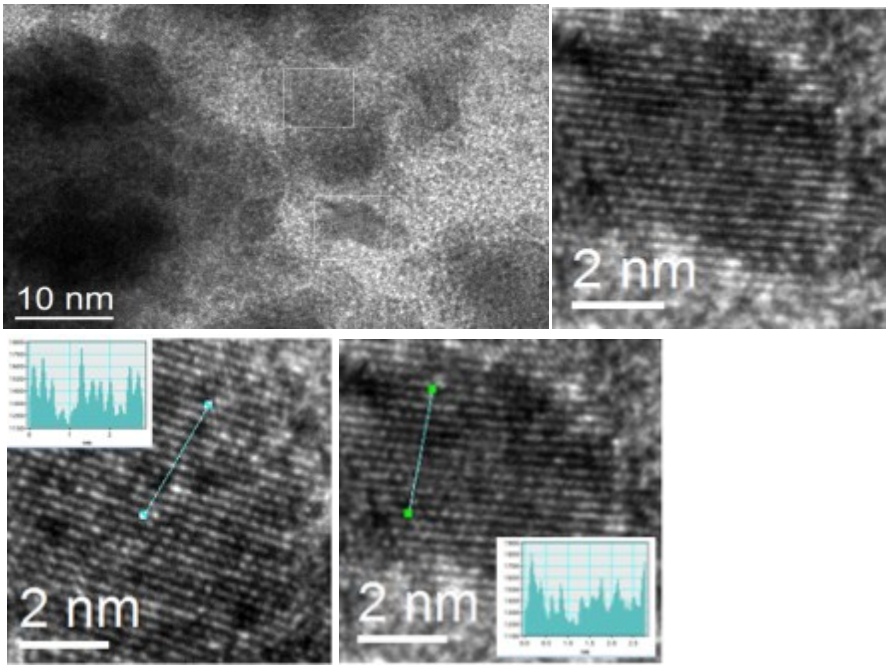

Ar-2-750°C-1hH_2

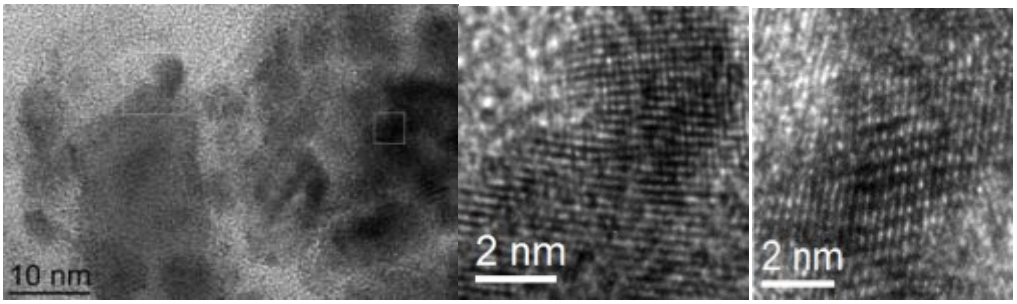

Ar-2-750°C-1hH_2

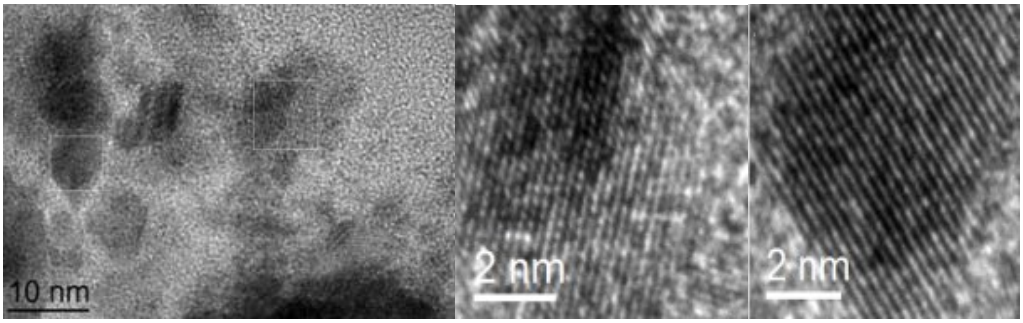

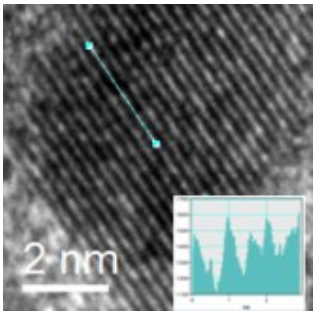

Ar-2-750°C-1hH_2

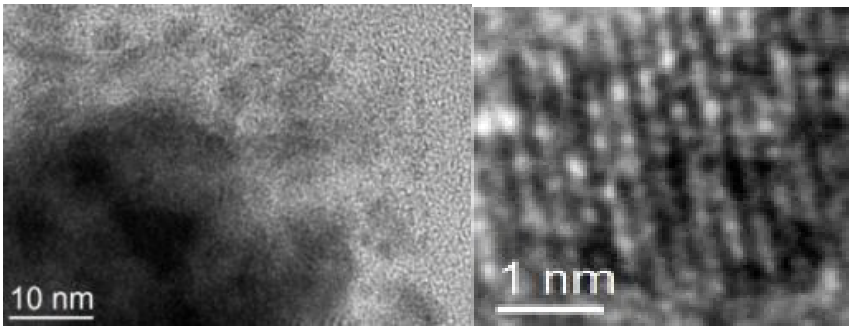

Ar-2-750°C-1hH_2

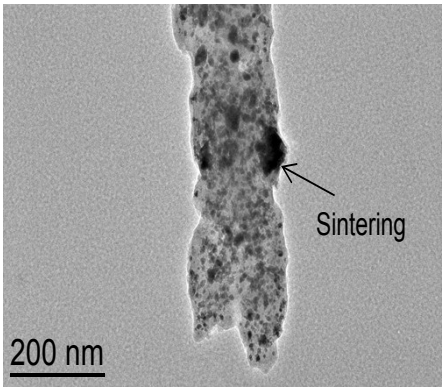

Ar-2-900°C-1h. Sintered particles are visible in the TEM images of Ar-2-900°C-1h.

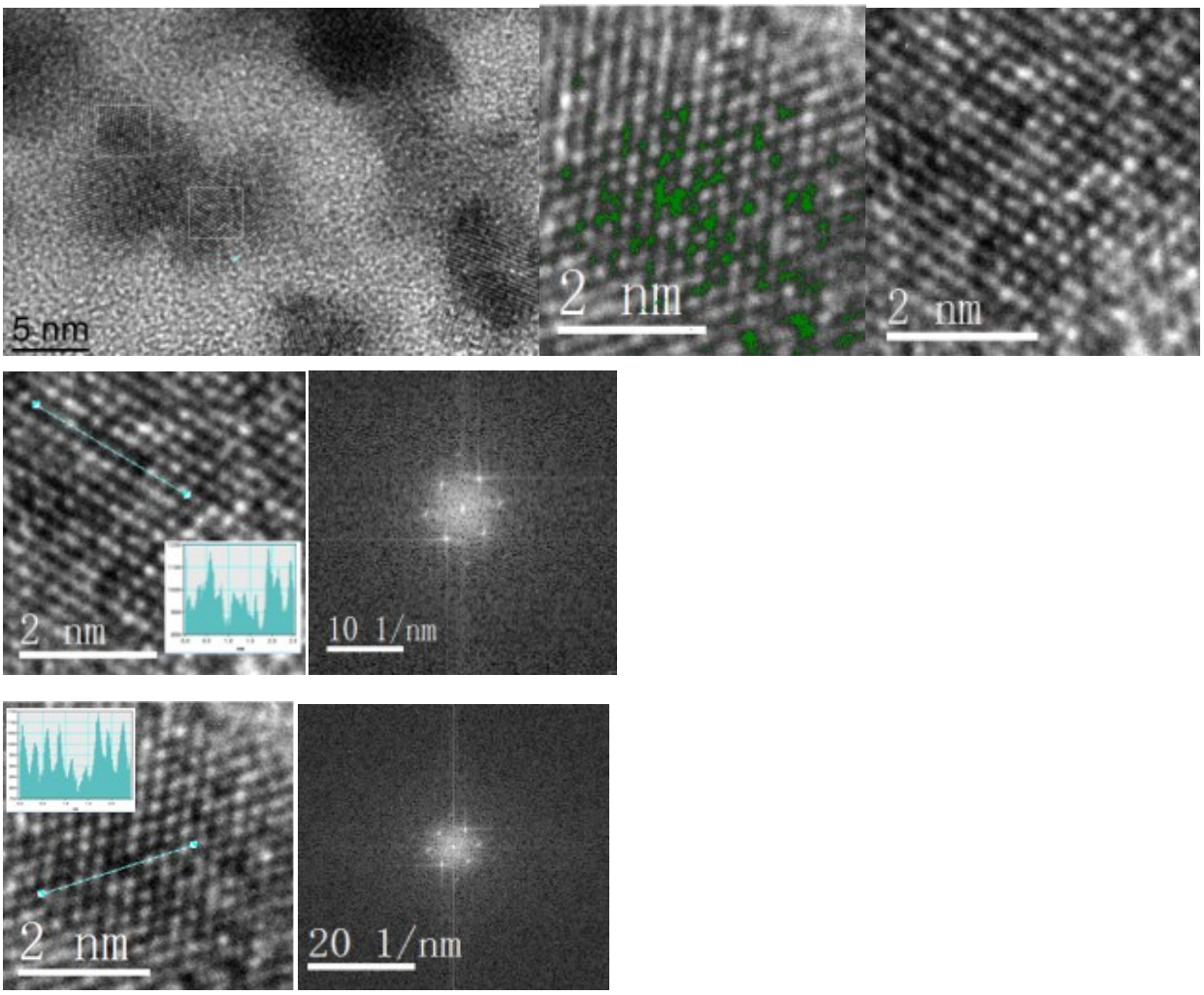

Ar-2-900°C-1h;

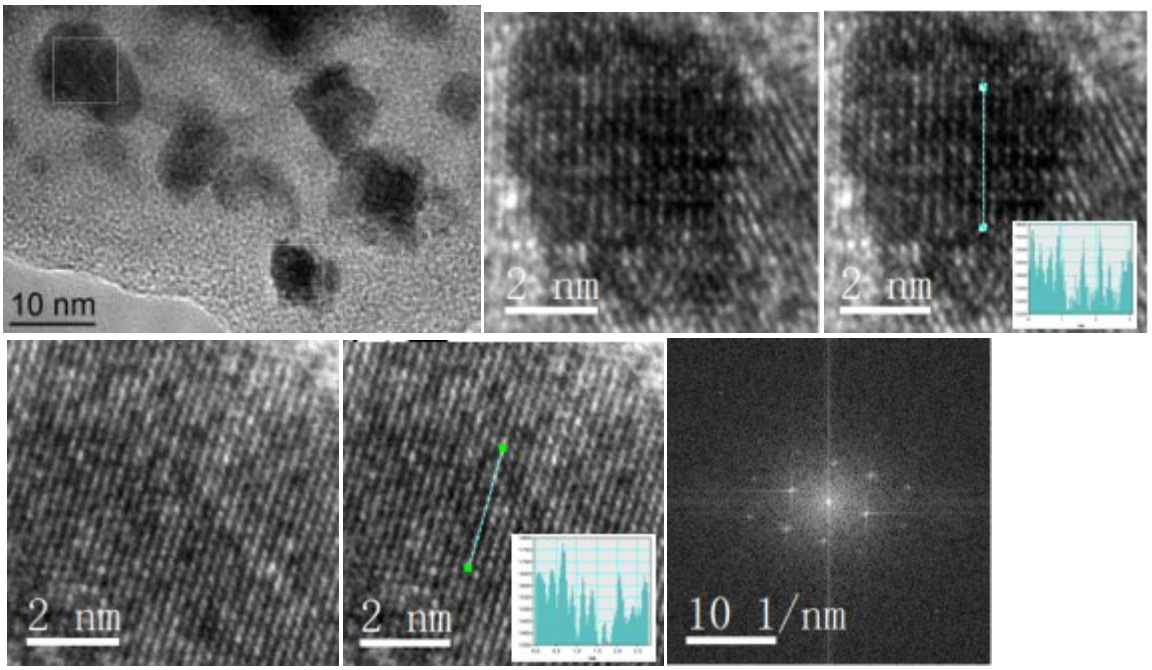

Ar-2-900°C-1h;

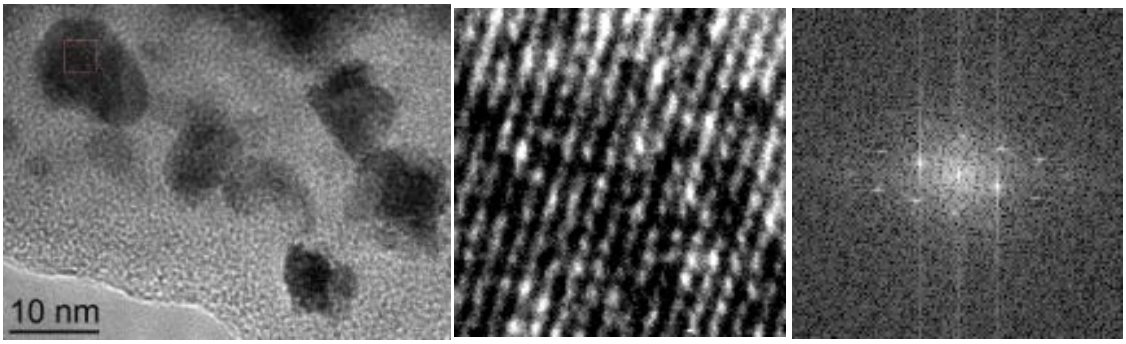

Ar-2-900°C-1h;

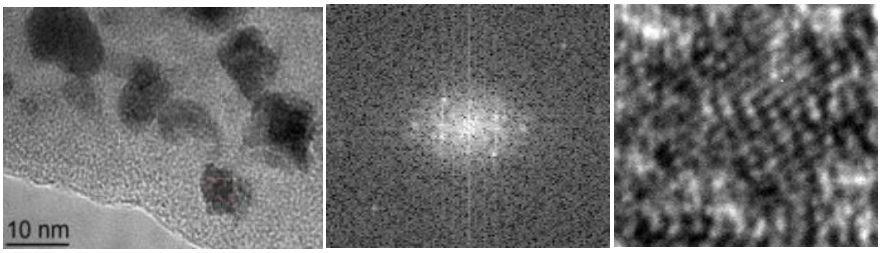

Ar-2-900°C-1h;

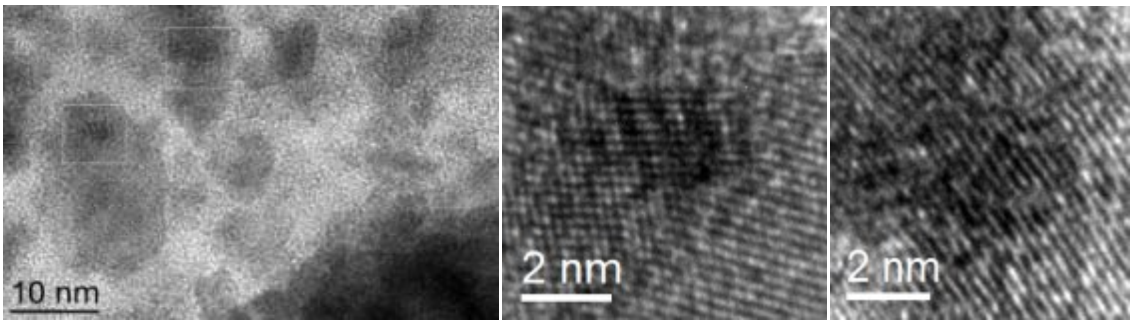

Ar-5-800°C-1h

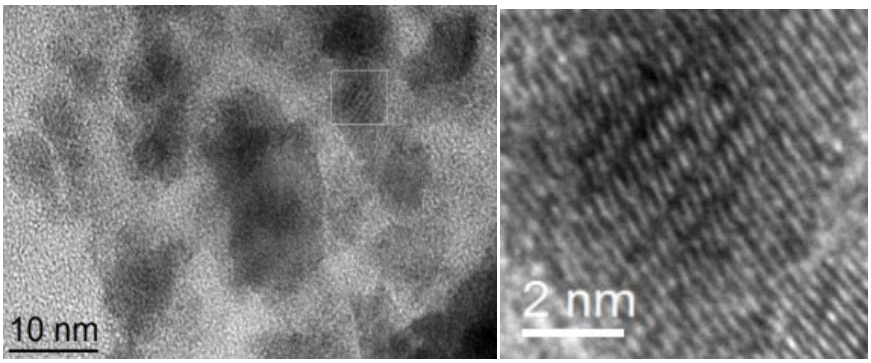

Ar-5-800°C-1h

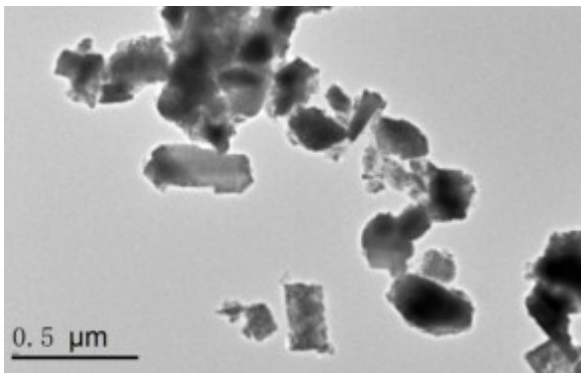

Ar-2-750°C-4h

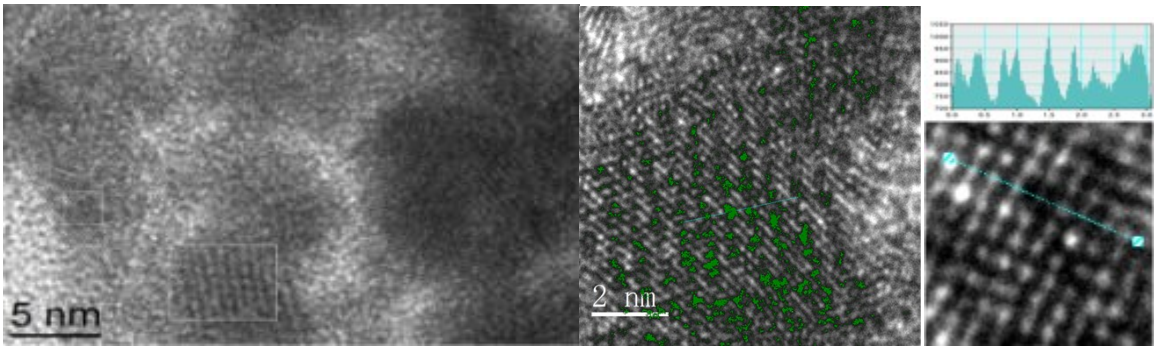

Ar-2-750°C-4h

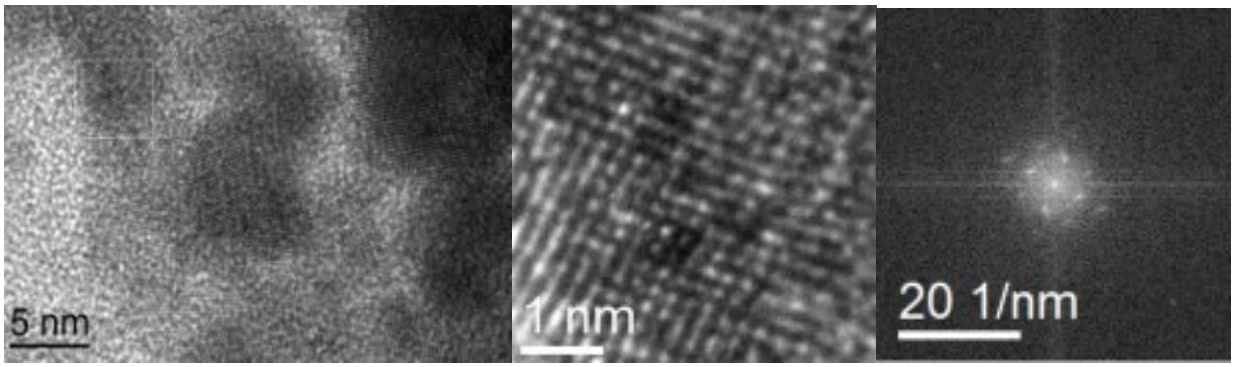

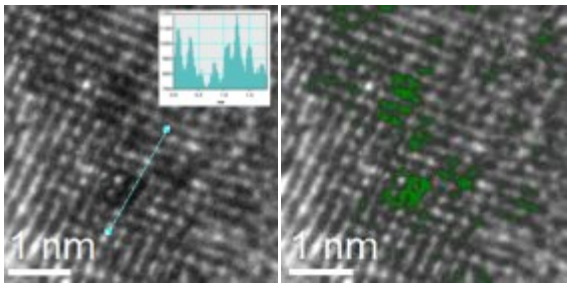

Ar-2-750°C-4h

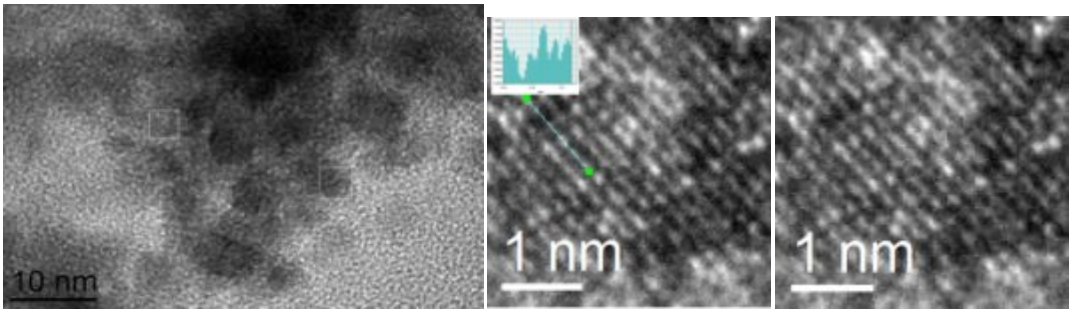

Ar-2-750°C-4h

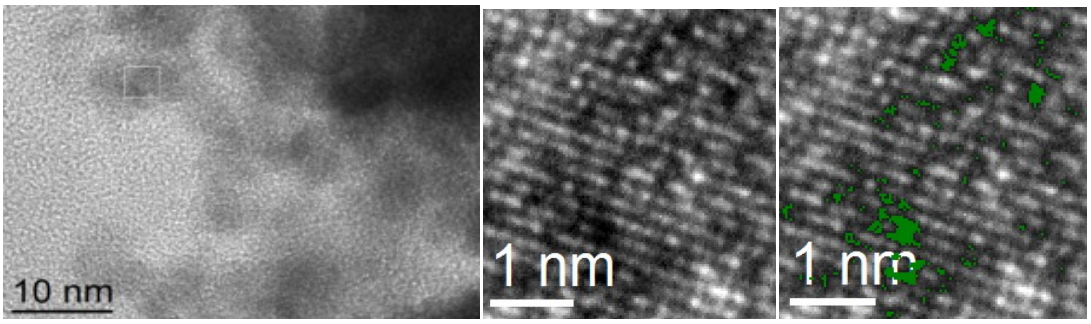

Ar-2-750°C-4h

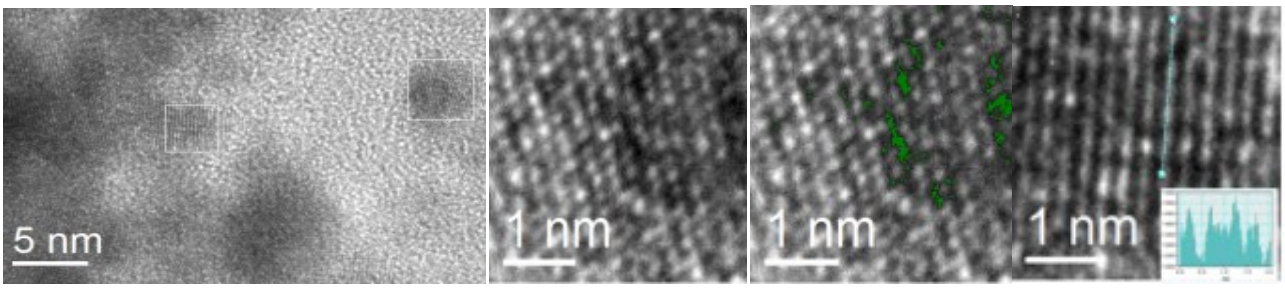

Ar-2-750°C-4h

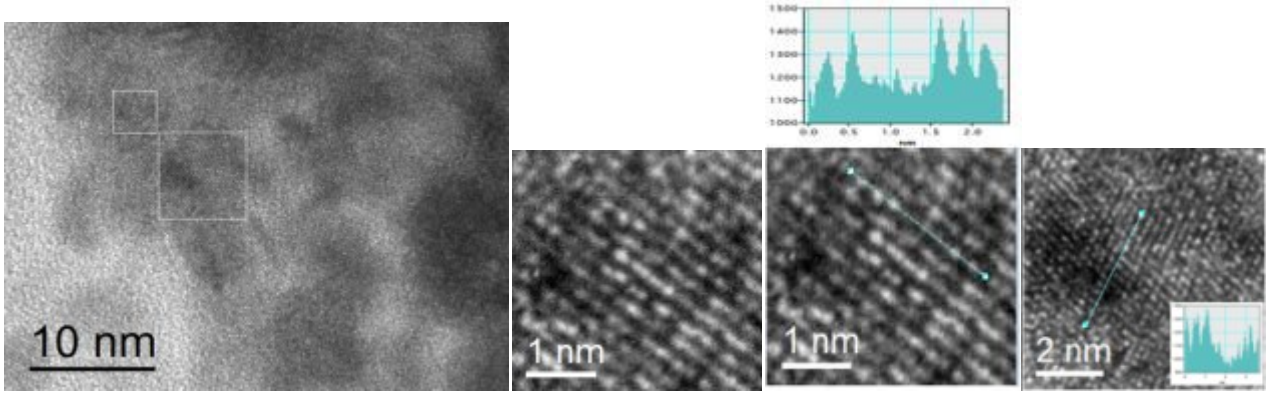

Ar-2-750°C-4h

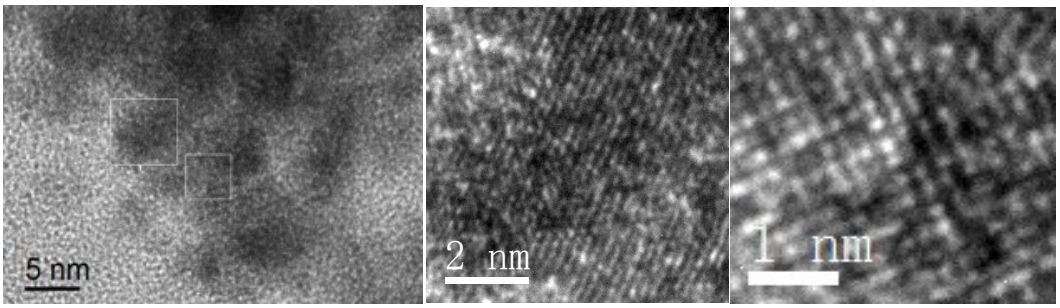

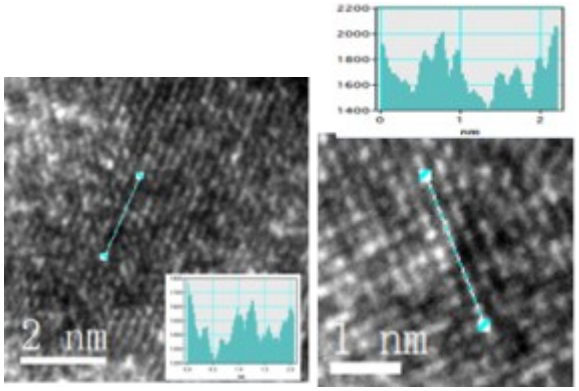

Ar-2-750°C-4h

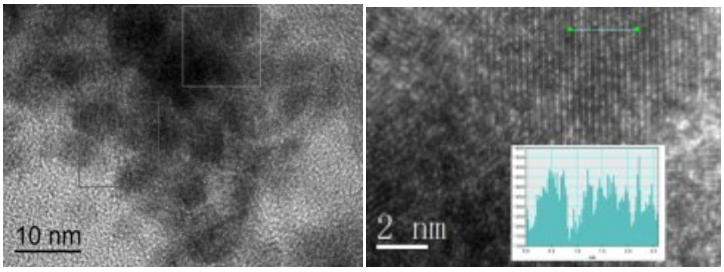

Ar-2-750°C-4h

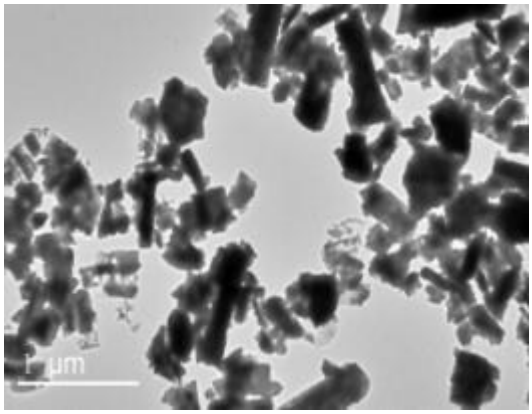

Ar-2-750°C-1h

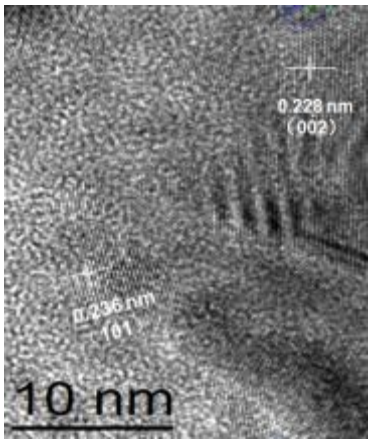

Ar-2-750°C-1h

The high-resolution TEM image of Ar-2-750°C-1h showed the analysis of a randomly selected region in which the lattice distances of 0.236 and 0.228 nm were indexed to the (002) and (101) facets, of W_2C with a hexagonal closed-packed structure.

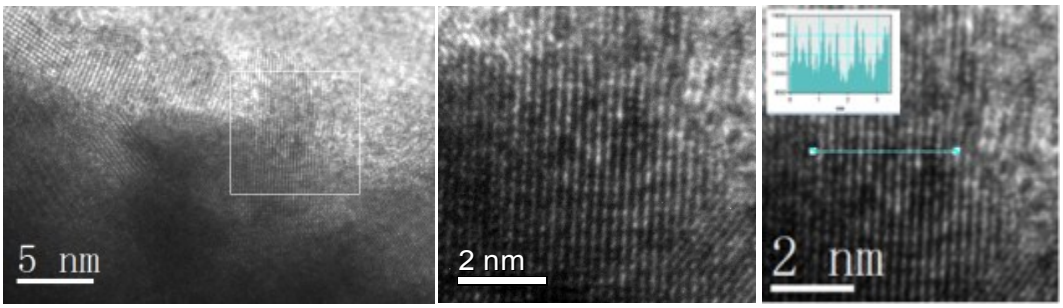

Ar-2-750°C-1h

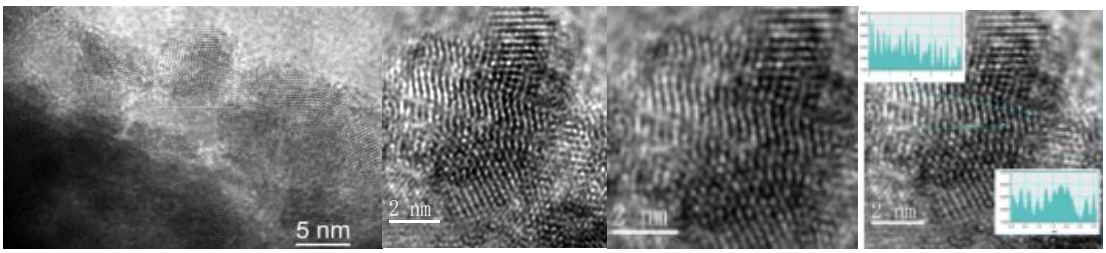

Ar-2-750°C-1h

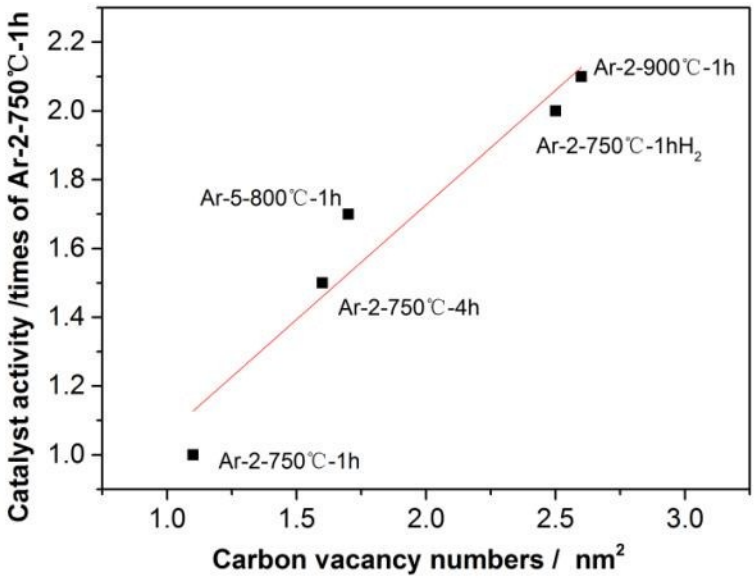

Figure S26. Relationship between catalytic activity and the numbers of carbon vacancies per square nanometers of the catalysts.

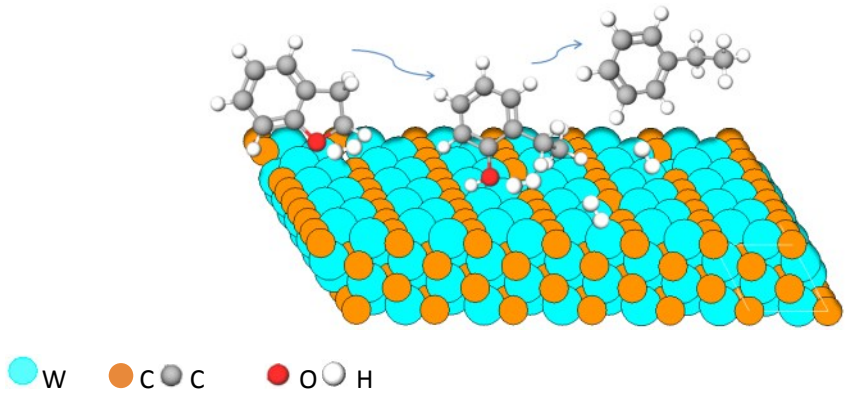

Figure S27. Proposed mechanism for hydrodeoxygenation of benzofuran on W2C with vacancy defects.

Weisz–Prater Criterion for Internal Diffusion[3]

Internal effectiveness factor for a first-order reaction in a spherical catalyst pellet

$$\eta = \frac{3}{\phi_1^2}(\phi_1 \coth\phi_1 - 1) \quad \text{(Eq-1)}$$

Weisz–Prater parameter:

$$C_{WP} = \eta\phi_1^2 = \frac{-r_A(obs)\rho_c R^2}{D_e C_{As}} \quad \text{(Eq-2)}$$

Where ρ_c=Density of catalyst particle, R = particle radius, De= Effective diffusivity, C_{As} = surface concentration

	Measuredrate(obs)[a] (mmol/（g_{cat}· s)× 10^3	PelletRadius(mm)
Run#1	1.502	0.19[b]
Run#2	1.551	0.05[c]

[a] Reactionconditions:T=350℃,P_{Total}=4MPa,W/F=1.218g_{cat}/(g_{BF}· h^{-1})

[b] Catalystparticlepreparedforthepurposeofmass-transferanalysis

[c] Thetypicalsizeofcatalystparticlesusedintheregularexperiment

Combining (Eq-1) and (Eq-2)

$$\frac{-r_A(obs)\rho_c R^2}{D_e C_{As}} = \eta\phi_1^2 = 3(\phi_1 \coth\phi_1 - 1) \quad \text{(Eq-3)}$$

Applying (Eq-3) to Runs#1 and #2, and take the ratio, then the terms ρ_c, De, and C_{As} cancel because the runs werecarried out under identical conditions.

$$\frac{-r_{A2}R_2^2}{-r_{A1}R_1^2} = \frac{\phi_{12}\coth\phi_{12} - 1}{\phi_{11}\coth\phi_{11} - 1} \quad \text{(Eq-4)}$$

The Thiele modulus:

$$\phi_1 = R\sqrt{\frac{-r_{As}\rho_c}{D_e C_{As}}} \quad \text{(Eq-5)}$$

Take the ratio of the Thiele modulus for Runs #1 and #2

$$\frac{\phi_{11}}{\phi_{12}} = \frac{R_1}{R_2} \quad \text{(Eq-6)}$$

or ϕ_{11}= (R_1/R_2)ϕ_{12}= (0.19mm)/(0.05mm)ϕ_{12}= 3.8ϕ_{12}(Eq-7)

Substituting for ϕ_{11} in (Eq-4) and evaluating -r_A and R for Runs#1 and #2

$$\left(\frac{1.551}{1.407}\right)\left(\frac{0.05^2}{0.19^2}\right) = 0.67 = \frac{\phi_{12}coth\phi_{12} - 1}{(3.8\ \phi_{12})coth(3.8\ \phi_{12}) - 1}$$

Solving this equation：

ϕ_{12}=0.12 for R_2= 0.05mm, then

ϕ_{11}= 3.8ϕ_{12}=0.456 for R_1= 0.19mm

Substituting for the obtained ϕ_{12} and ϕ_{11} in (Eq-1) and evaluating the corresponding effectiveness factors

For R_2:

$$\eta = \frac{3}{{\phi_{12}}^2}\left(\phi_{12} coth \phi_{12} - 1\right) = \frac{3}{0.12^2}(0.12 coth(0.12) - 1) = 0.999$$

For R_1:

$$\eta = \frac{3}{{\phi_{11}}^2}\left(\phi_{11} coth \phi_{11} - 1\right) = \frac{3}{0.456^2}(0.456 coth(0.456) - 1) = 0.986$$

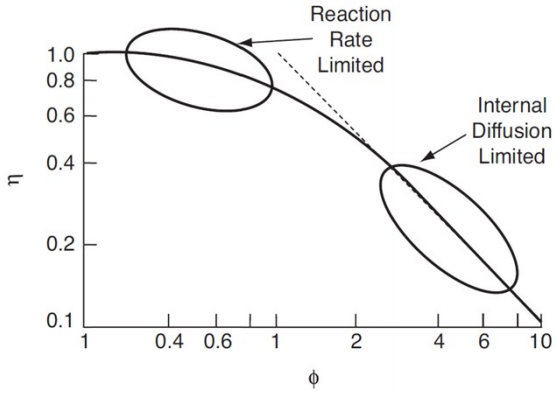

The typical size of catalyst particles used in this work is0.05mm. The corresponding effectivenessfactors suggest that the reaction is not controlled by the internal diffusion (i.e., η>0.95).

References

(1) Yu-Ran Luo-Comprehensive Handbook of Chemical Bond Energies-CRC Press (2007).

(2) Liu, C. Y.; Shao, Z. F.; Xiao, Z. H.; Williams, C. T.; Liang, C. H. *Energy & Fuels* 2012, *26*, 4205.

(3) H. S. Fogler, "Elements of Chemical Reaction Engineering". Printice- Hall International Editions, (1987).